engineering proceedings

MDPI

Proceeding Paper

Spatial Structure Analysis for Subsurface Defect Detection in Materials Using Active Infrared Thermography and Adaptive Fixed-Rank Kriging †

Chun-Han Chang [1], Stefano Sfarra [2], Nan-Jung Hsu [3] and Yuan Yao [1,*]

[1] Department of Chemical Engineering, National Tsing Hua University, Hsinchu 300044, Taiwan; gray25905634@gmail.com
[2] Department of Industrial and Information Engineering and Economics, University of L'Aquila, 67100 L'Aquila, Italy; stefano.sfarra@univaq.it
[3] Institute of Statistics, National Tsing Hua University, Hsinchu 300044, Taiwan; njhsu@stat.nthu.edu.tw
* Correspondence: yyao@mx.nthu.edu.tw
† Presented at the 17th International Workshop on Advanced Infrared Technology and Applications, Venice, Italy, 10–13 September 2023.

Abstract: The study focuses on reducing noise and nonstationary backgrounds in data collected through active infrared thermography (AIRT) for defect detection in materials. The authors employ adaptive fixed-rank kriging to analyze a sequence of thermograms obtained in the AIRT experiment. Using basis functions derived from thin-plate splines, the data features are represented at various resolution levels, resulting in a concise spatial covariance function representation. Eigenfunctions are then derived from the estimated covariance function to capture spatial structures at different scales. Visualizing these eigenfunctions highlights defect information. The authors validate their approach through a pulsed thermography experiment on a carbon-fiber-reinforced plastic (CFRP) sample, demonstrating its effectiveness in detecting defects.

Keywords: thermographic data processing; active thermography; adaptive fixed-rank kriging; defect detection

Citation: Chang, C.-H.; Sfarra, S.; Hsu, N.-J.; Yao, Y. Spatial Structure Analysis for Subsurface Defect Detection in Materials Using Active Infrared Thermography and Adaptive Fixed-Rank Kriging. *Eng. Proc.* **2023**, *51*, 43. https://doi.org/10.3390/engproc2023051043

Academic Editors: Gianluca Cadelano, Giovanni Ferrarini and Davide Moroni

Published: 14 December 2023

1. Introduction

Nondestructive testing (NDT) techniques have gained popularity in various applications, particularly for examining high-value materials. Active infrared thermography (AIRT) is a commonly used NDT technique due to its convenience and rapid testing capabilities. Researchers have applied AIRT in different contexts, such as defect detection in carbon-fiber-reinforced thermoplastic samples [1]. However, a common challenge in AIRT inspection is dealing with heavily polluted raw data, which often contain non-uniform backgrounds and noise. This necessitates appropriate signal preprocessing methods to extract the underlying information, specifically the defect signals. Among the various existing methods, one practical approach is principal component thermography (PCT) [2]. PCT utilizes principal component analysis to extract features from thermographic data through eigenvalue decomposition. However, it is worth noting that while PCT reduces the dimensionality of the data, it does not explicitly eliminate noise, although some portion of the noise may be attenuated during the process of dimensionality reduction.

In this study, we propose the use of a spatial statistical method called adaptive fixed-rank kriging (autoFRK) for thermographic data processing. Kriging is a methodology that can estimate the covariance function and generate optimal predictions from a sequence of independent, incomplete, and noisy spatial data. However, kriging involves the computation of inverse covariance matrices, which can be challenging when dealing with massive spatial datasets. Furthermore, the thermograms obtained in our experiment often exhibited heterogeneity, and the locations of defects were frequently unknown. These uncertainties

pose challenges and make traditional kriging methods less applicable. To address these issues, we adopt fixed-ranked kriging, initially proposed by Cressie and Johannesson [3], which tackles the problems associated with large spatial datasets and heterogeneity in the data. Specifically, we employ autoFRK proposed by Tzeng and Huang [4]. AutoFRK is an automatic process that eliminates the need for miscellaneous parameter tuning and is computationally efficient. In our applications, the original thermograms are represented using a set of basis functions ordered by the resolution level, where different component levels represent distinct scales of the estimated features. These basis functions form the spatial covariance function, from which the eigenfunctions encoding the spatial structure are obtained. Defect information can be highlighted by visualizing the eigenfunctions.

2. Methodology

2.1. Specimen and Experiment

In the experiment, the CFRP specimen was fabricated using the vacuum-assisted resin transfer molding (VARTM) technique. Multiple layers of carbon fiber sheets were applied to strengthen the specimen, with each sheet having a thickness of 0.26 cm. Before executing VARTM, nine Teflon square strips with different areas were inserted into the fiber sheets to simulate defects. The side lengths of these defects were 1.6 cm, 0.8 cm, and 0.4 cm, respectively. Additionally, a rectangular defect measuring 1.4 cm × 0.6 cm was created using insulating tape. In total, the CFRP specimen contained ten defective regions. The four shallowest defects were covered by a single layer of carbon fiber sheet, while two layers of sheets covered three defects, and the three deepest defects were covered by three layers of sheets. As a result, these defects were located at different depths and were not visible to the naked eye after resin infiltration. To detect defects, pulsed thermography was employed in the experiment. The procedure involved heating the specimen using a thermal pulse generated from a flash source. Subsequently, an NEC infrared camera of type TAS-G100EXD was utilized to capture a sequence of thermograms, enabling the collection of thermographic data. A total of 59 thermograms were recorded. Figure 1 illustrates some of these images, where only the shallowest defects are visible. In these figures, the numbers on the color bars represent the pixel values.

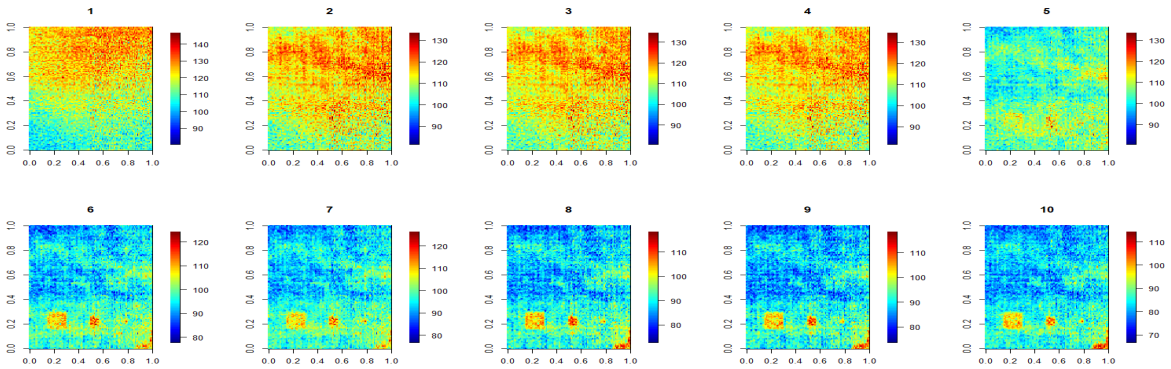

Figure 1. The first 10 frames of thermograms collected in the experiment.

2.2. Adaptive Fixed-Ranked Kriging

AutoFRK is a method designed to enhance the handling of massive datasets in the regular FRK framework by automating the process. The autoFRK model relies on a set of basis functions derived from thin-plate splines (TPS). Let us consider a set of observed thermogram data $\boldsymbol{z}_t \equiv (z(\boldsymbol{s}_1, t), \ldots, z(\boldsymbol{s}_n, t))'$, where frames are captured at $t = 1, \ldots, T$, with $T \geq 1$, and at n distinct pixels. $\boldsymbol{s}_1, \ldots, \boldsymbol{s}_n$ are vectors containing spatial coordinate information. We assume a spatial process, $\{y(\boldsymbol{s}, t) : \boldsymbol{s} \in \mathbb{R}^2\}; t = 1, \ldots, T$, with a mean

$\mu(\boldsymbol{s},t)$ and a spatial covariance function $C(\boldsymbol{s},\boldsymbol{s}^*) = cov(y(\boldsymbol{s},t),\ y(\boldsymbol{s}^*,t))$. The relationship between the observed data and the spatial process is given by

$$\boldsymbol{z}_t = \boldsymbol{y}_t + \boldsymbol{\varepsilon}_t; \quad t = 1,\ \ldots,\ T \tag{1}$$

where $\boldsymbol{\varepsilon}_t \sim N\left(\boldsymbol{0}, \sigma_\varepsilon^2 \boldsymbol{I}_n\right)$ represents additive white noise, $\boldsymbol{y}_t \equiv (y(\boldsymbol{s}_1,t),\ldots,y(\boldsymbol{s}_n,t))'$. To estimate the covariance function $C(\boldsymbol{s},\boldsymbol{s}^*)$ based on $\boldsymbol{z}_1,\ \ldots,\ \boldsymbol{z}_T$, the spatial random effects model of $y(\boldsymbol{s},t)$ is defined as

$$y(\boldsymbol{s},t) = \mu(\boldsymbol{s},t) + \boldsymbol{w}_t'\boldsymbol{f}(\boldsymbol{s}) + \xi(\boldsymbol{s},t) = \mu(\boldsymbol{s},t) + \sum_{k=1}^{K} w_k(t) f_k(\boldsymbol{s}) + \xi(\boldsymbol{s},t) \tag{2}$$

where $\{f_k(\boldsymbol{s}) : k = 1,\ \ldots,\ K\}$ are prespecified basis functions at K different resolution levels, with $K \leq n$. $\boldsymbol{f}(\boldsymbol{s}) = (f_1(\boldsymbol{s}),\ \ldots,\ f_K(\boldsymbol{s}))\prime$ represents the basis function vector, $\boldsymbol{w}_t = (w_1(t),\ \ldots,\ w_K(t))' \sim N(0,\boldsymbol{M})$ represents the random effects, $\boldsymbol{M}$ is an unknown nonnegative-definite matrix, and $\xi(\boldsymbol{s},t) \sim N\left(0,\sigma_\xi^2\right)$ is a white-noise process. The corresponding spatial covariance function is given by

$$C(\boldsymbol{s},\boldsymbol{s}^*) = cov(y(\boldsymbol{s},t),y(\boldsymbol{s}^*,t)) = \boldsymbol{f}(\boldsymbol{s})'\boldsymbol{M}\boldsymbol{f}(\boldsymbol{s}^*) + \sigma_\xi^2 I(\boldsymbol{s}=\boldsymbol{s}^*); \boldsymbol{s},\boldsymbol{s}^* \in \mathbb{R}^2 \tag{3}$$

where $I(\boldsymbol{s}=\boldsymbol{s}^*) = 1$ if $\boldsymbol{s}=\boldsymbol{s}^*$ and 0 otherwise.

In autoFRK, the basis functions $\boldsymbol{f}(\boldsymbol{s})$ are constructed using TPS. The resulting basis functions, referred to as multiresolution thin-plate spline basis functions, are defined as

$$f_k(\boldsymbol{s}) = \begin{cases} 1; & k = 1, \\ x_{k-1}; & k = 2,\ldots,d+1\,, \\ \lambda_{k-d-1}^{-1}\left\{\boldsymbol{\phi}(\boldsymbol{s}) - \boldsymbol{\Phi}\boldsymbol{X}(\boldsymbol{X}'\boldsymbol{X})^{-1}\boldsymbol{x}\right\}\prime \boldsymbol{v}_{k-d-1}; & k = d+2,\ldots,n. \end{cases} \tag{4}$$

Here, $\boldsymbol{x} = (1,\boldsymbol{s}')' = (1,x_1,x_2)'$ with x_1, x_2 being the spatial coordinate indices, $\boldsymbol{\phi}(\boldsymbol{s}) = (\phi_1(\boldsymbol{s}),\ldots,\phi_n(\boldsymbol{s}))'$ with

$$\phi_i(\boldsymbol{s}) = \begin{cases} \frac{1}{12}\|\boldsymbol{s}-\boldsymbol{s}_i\|^3; & d = 1, \\ \frac{1}{8\pi}\|\boldsymbol{s}-\boldsymbol{s}_i\|^2 \log\left(\|\boldsymbol{s}-\boldsymbol{s}_i\|\right); & d = 2, \\ \frac{1}{8}\|\boldsymbol{s}-\boldsymbol{s}_i\|; & d = 3. \end{cases} \tag{5}$$

$$\boldsymbol{\Phi} = \begin{pmatrix} \phi_1(\boldsymbol{s}_1) & \cdots & \phi_n(\boldsymbol{s}_1) \\ \vdots & \ddots & \vdots \\ \phi_1(\boldsymbol{s}_n) & \cdots & \phi_n(\boldsymbol{s}_n) \end{pmatrix},\ \boldsymbol{X} = \begin{pmatrix} 1 & x_{11} & x_{12} \\ \vdots & \vdots & \vdots \\ 1 & x_{n1} & x_{n2} \end{pmatrix} \tag{6}$$

Define $\boldsymbol{Q} = \boldsymbol{I} - \boldsymbol{X}(\boldsymbol{X}'\boldsymbol{X})^{-1}\boldsymbol{X}'$, $\boldsymbol{v}_k$ represents the kth column of $\boldsymbol{V}$, where $\boldsymbol{V}\text{diag}(\lambda_1,\ldots,\lambda_n)\boldsymbol{V}'$ is the eigen-decomposition of $\boldsymbol{Q}\boldsymbol{\Phi}\boldsymbol{Q}$.

Given the basis functions, $\boldsymbol{M}$ and σ_ξ^2 are estimated by the maximum likelihood estimates as the following forms:

$$\hat{\boldsymbol{M}}_K = \left(\boldsymbol{F}_K'\boldsymbol{F}_K\right)^{-1/2}\boldsymbol{P}_K\text{diag}\left(\hat{d}_{K,1},\ldots,\hat{d}_{K,K}\right)\boldsymbol{P}_K'\left(\boldsymbol{F}_K'\boldsymbol{F}_K\right)^{-\frac{1}{2}}, \tag{7}$$

$$\hat{\sigma}_{\xi,K}^2 = \max\left\{\frac{1}{n-L^*}\left(\text{tr}\left(\boldsymbol{S} - \sum_{k=0}^{L^*} d_{K,k}\right) - \sigma_\epsilon^2, 0\right\}\right. . \tag{8}$$

Here, $\boldsymbol{S} = \frac{1}{T}\sum_{t=1}^{T}\boldsymbol{z}_t\boldsymbol{z}_t'$, $\boldsymbol{F}_K = (\boldsymbol{f}_1,\ldots,\boldsymbol{f}_K)$, and $\boldsymbol{f}_k = (f_k(\boldsymbol{s}_1),\ldots,f_k(\boldsymbol{s}_n))'$, $k = 1,\ldots,K$. $\boldsymbol{P}_K\text{diag}(d_{K,1},\ldots,d_{K,K})\boldsymbol{P}_K'$ represents the eigen-decomposition of $\left(\boldsymbol{F}_K'\boldsymbol{F}_K\right)^{-1/2}\boldsymbol{F}_K'\boldsymbol{S}\boldsymbol{F}_K\left(\boldsymbol{F}_K'\boldsymbol{F}_K\right)^{-1/2}$. The value of $\hat{d}_{K,k}$ is obtained as $\max\left(d_{K,k} - \hat{\sigma}_{\xi,K}^2 - \sigma_\epsilon^2, 0\right)$, with $d_{K,0} = 0$. L^* is the largest $L \in \{1,\ldots,K\}$ such that $d_{K,L} > \max\left\{\frac{1}{n-L}\left(\text{tr}(\boldsymbol{S}) - \sum_{k=1}^{L} d_{K,k}, \sigma_\epsilon^2\right\}\right.$ if it exists; otherwise, it is 0.

Once the basis functions $\boldsymbol{f}(\boldsymbol{s})$ are specified and $\boldsymbol{M}$ is estimated, the corresponding covariance function is obtained as

$$\hat{C}(\boldsymbol{s}, \boldsymbol{s}^*) = \boldsymbol{f}(\boldsymbol{s})' \hat{\boldsymbol{M}}_K \boldsymbol{f}(\boldsymbol{s}^*) \tag{9}$$

Furthermore, the eigenfunction of the spatial covariance function is given by

$$F_k(s) = \boldsymbol{f}(\boldsymbol{s})' \hat{\boldsymbol{M}}_K \boldsymbol{f}(\boldsymbol{s}^*) \boldsymbol{\lambda}_k \tag{10}$$

where $\boldsymbol{\lambda}_k$ represents the kth eigenvector of $\hat{C}(\boldsymbol{s}, \boldsymbol{s}^*)$, and k ranges from 1 to n. The resulting eigenfunctions are then visualized for observation.

3. Results

In the case study, every fifth frame of the thermograms was subjected to autoFRK and decomposed at a resolution level $k = 300$. The first two eigenfunctions resulting from this decomposition are shown in Figure 2. The first eigenfunction focuses on the nonuniform background caused by uneven heating. In addition, the shallow defects can also be observed. The second eigenfunction still captures the shallow defects. Additionally, deeper defects become visible in this eigenfunction. The subsequent eigenfunctions, which are not shown in this paper, mainly reflect noise.

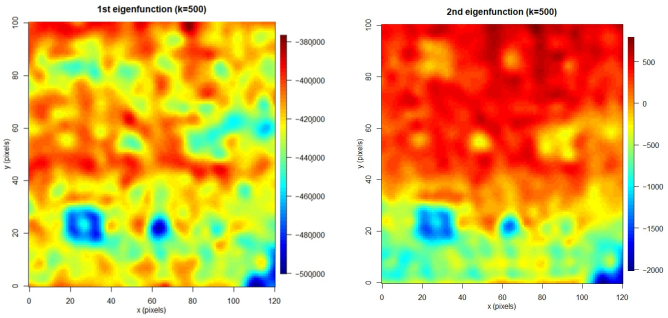

Figure 2. The first two eigenfunctions derived from autoFRK.

4. Conclusions

In this article, the authors propose the adoption of autoFRK to enhance AIRT-based defect detection in high-valued materials. By utilizing autoFRK, it is possible to model the sequence of thermographic data. The results obtained from autoFRK highlight features at different levels, facilitating a more comprehensive examination of the defects present.

Author Contributions: Conceptualization, N.-J.H. and Y.Y.; methodology, N.-J.H. and Y.Y.; software, C.-H.C.; validation, S.S.; formal analysis, C.-H.C.; investigation, C.-H.C.; resources, S.S.; data curation, Y.Y.; writing—original draft preparation, C.-H.C.; writing—review and editing, S.S., N.-J.H. and Y.Y.; visualization, C.-H.C.; supervision, Y.Y.; project administration, Y.Y.; funding acquisition, N.-J.H., S.S. and Y.Y. All authors have read and agreed to the published version of the manuscript.

Funding: This research was funded by the National Science and Technology Council, ROC, grant number NSTC 111-2634-F-007-010, and UNIVAQ RIA research funds 2023.

Institutional Review Board Statement: Not applicable.

Informed Consent Statement: Not applicable.

Data Availability Statement: The data presented in this study are available on request from the corresponding author.

Conflicts of Interest: The authors declare no conflict of interest.

References

1. Liu, K.; Zheng, M.; Liu, Y.; Yang, J.; Yao, Y. Deep autoencoder thermography for defect detection of carbon fiber composites. *IEEE Trans. Ind. Inform.* **2023**, *19*, 6429–6438. [CrossRef]
2. Rajic, N. Principal component thermography for flaw contrast enhancement and flaw depth characterisation in composite structures. *Compos. Struct.* **2002**, *58*, 521–528. [CrossRef]
3. Cressie, N.; Johannesson, G. Fixed rank Kriging for very large data sets. *J. R. Stat. Soc. Ser. B* **2008**, *70*, 209–226. [CrossRef]
4. Tzeng, S.; Huang, H.-C. Resolution adaptive fixed rank Kriging. *Technometrics* **2018**, *60*, 198–208. [CrossRef]